Environmental Science Advances

ROYAL SOCIETY OF CHEMISTRY

PAPER

View Article Online
View Journal | View Issue



Cite this: *Environ. Sci.: Adv.*, 2022, **1**, 331

# Ultra-fast $^{137}$Cs sequestration *via* a layered inorganic indium thioantimonate†

Xi Zeng,[ab] Min Zeng,[c] Ping-Wei Cai,[ab] Jun-Hao Tang,[ab] Wen Ma,[ab] Mei-Ling Feng *[ab] and Xiao-Ying Huang[ab]

As a non-actinide fission product of uranium, $^{137}$Cs has a long half-life, high-energy γ-ray emissions, and facile accessibility to ecosystems due to the high solubility and mobility of $Cs^+$ ions. Hence, rapid remediation of $^{137}$Cs from radioactive wastewater is an urgent task. Here, we have developed a layered inorganic indium thioantimonate $K_2In_2Sb_2S_7{\cdot}2.2H_2O$ (KIAS) prepared *via* cationic substitution from $[(CH_3)_2NH_2]_2In_2Sb_2S_7$ (NIAS) for the efficient enrichment and sequestration of $Cs^+$ from complex aqueous solutions. KIAS possesses excellent radiation resistance, hydrolytic stability ($In^{3+}$ leaching rates ≤ 0.01% at pH 1–13) and high $Cs^+$ adsorption activity. Compared to unactivated NIAS, KIAS has enlarged interlayer spacing and exchangeable interlayer $K^+$ ions. It exhibits extremely fast adsorption kinetics towards $Cs^+$ with high removal rate (~93%) in only 1 min, a record for $Cs^+$ adsorbents. It also displays high adsorption capacity (309.60 mg $g^{-1}$) and outstanding selectivity for $Cs^+$ under the interference of large amounts of alkali (earth) metal ions, anions, and humic acid and even in actual tap water or lake water. Furthermore, KIAS can reversibly trap and release $Cs^+$ ions for at least five adsorption–desorption cycles in an easy-to-operate and environmentally friendly elution procedure. The adsorption mechanism of $Cs^+$ on KIAS, revealed by batch adsorption experiments and characterizations, is ion exchange between $Cs^+$ and interlayer $K^+$ ions. This work not only highlights KIAS as a promising $Cs^+$ scavenger to minimize contamination in complicated wastewater, but also presents a cation activation strategy to greatly enhance the adsorption performance of layered metal sulfides.

Received 4th April 2022
Accepted 7th June 2022

DOI: 10.1039/d2va00060a

rsc.li/esadvances



### Environmental significance

$^{137}$Cs possesses a long half-life and strong γ-ray radiation emissions, posing serious threats to human health and environmental safety. It remains a serious challenge to efficiently capture $^{137}$Cs from radioactive wastewater due to its high solubility and easy mobility, and the influence of interfering ions. This study achieves ultra-fast and selective sequestration of $Cs^+$ from complicated aqueous solutions through the ion exchange method by employing a layered inorganic indium thioantimonate, $K_2In_2Sb_2S_7{\cdot}2.2H_2O$ (KIAS), which is prepared *via* cationic substitution from $[(CH_3)_2NH_2]_2In_2Sb_2S_7$ (NIAS). This work not only demonstrates that KIAS has excellent application potential for highly efficient incarceration of $Cs^+$ from wastewater, but also presents a cation activation strategy to greatly enhance the adsorption performance of layered metal sulfides.

## 1 Introduction

Over the past decades, radionuclides such as $^{134}$Cs, $^{137}$Cs, $^{90}$Sr and $^{131}$I have been released into the environment following nuclear power activities, nuclear accidents, and nuclear weapons tests, causing irreversible damage to the ecological environment and human health.[1] Among these radionuclides, $^{137}$Cs, one of the main fission products of $^{235}$U, is the most hazardous radionuclide with high fission yields (6.18%), long half-life (30.17 years) and strong γ-ray radiation emissions.[2] Furthermore, the high solubility and mobility of $Cs^+$ cause its easy migration and diffusion into aqueous systems.[3] Radioactive $^{137}$Cs can accumulate in living organisms, thereby posing a serious threat to human health, such as cancer, genetic disorders, genetic mutation, and other diseases.[4,5] On the other hand, the concentrations of non-radioactive competing ions (*e.g.* $Na^+$, $K^+$, $Mg^{2+}$, $Ca^{2+}$) coexisting in various radioactive wastewaters are usually much higher than that of $Cs^+$, which can inhibit the uptake of $^{137}$Cs.[6] Accordingly, the rapid and selective removal of $^{137}$Cs from nuclear wastewater is essential and urgent.

Many treatment methods such as membrane separation,[7] chemical precipitation,[8] solvent extraction,[9] nanofiltration,[10]

[a]State Key Laboratory of Structural Chemistry, Fujian Institute of Research on the Structure of Matter, Chinese Academy of Sciences, Fuzhou 350002, P. R. China. E-mail: fml@fjirsm.ac.cn
[b]University of Chinese Academy of Sciences, Beijing 100049, P. R. China
[c]Hubei Key Laboratory of Ferro- & Piezoelectric Materials and Devices, Faculty of Physics and Electronic Science, Hubei University, Wuhan 430062, China

† Electronic supplementary information (ESI) available. See https://doi.org/10.1039/d2va00060a

ultrafiltration,[11] adsorption[12] and ion exchange[13,14] have been utilized to remediate $Cs^+$ contaminated wastewater. Of these methods, ion exchange has attracted widespread attention due to its simple and flexible operation, well-established technology, high separation efficiency, and minimum solidified wastes.[15–17] In comparison with organic ion exchangers, the inorganic ones exhibit lower production costs, higher thermal, chemical and ionizing radiation stabilities, and higher selectivities for specific ions, and thus have become a hotspot of research over the past decades.[18,19] Additionally, in contrast to natural non-homogeneous adsorbents such as clays and zeolites, synthetic inorganic ion exchangers may be fabricated with a well-defined phase and chemical composition, and possess tunable characteristics such as particle shape, size and porosity as well as high adsorption capacity.[20] However, previous $Cs^+$ ion-exchangers often suffered from slow adsorption rate, low adsorption capacity, and poor selectivity or renewability.

Metal sulfides have become a new growing class of ion exchangers, showing fast adsorption kinetics and exceptional selectivity for soft or relatively soft metal ions.[21–23] These can be justified by the following reasons: (i) the $S^{2-}$ ligand in the framework belongs to Lewis soft base with an innately strong affinity for Lewis soft acids;[14,24] (ii) the flexible chemical bonding and open-framework allow the target ions to be "locked" by the "breathing effect" during ion exchange.[25,26] Recent advances in the capture of $Cs^+$ ions have been focused on layered metal sulfides characterized by flexible interlayer spaces, large specific surface area, many exposed $S^{2-}$ adsorption sites and labile interlayer cations, which facilitate easy diffusion of external $Cs^+$ ions and thus exhibit fast adsorption kinetics.[13,14,24,26–28] Although great progress has been made in recent years, most of the available layered metal sulfides still have some problems during ion exchange, for example, the release of environmentally unfriendly organic amines from $[(CH_3)_2NH_2]_2Ga_2Sb_2S_7\cdot H_2O$ and FJSM-SnS,[13,26] and the oxidation of $Mn^{2+}$ to $Mn^{3+}$ in KMS-1 resulting in a lower than theoretical adsorption capacity for $Cs^+$ ions.[24] Therefore, increasing efforts have been made to develop environmentally friendly and chemically stable inorganic layered metal sulfide-based exchangers with high adsorption performance for the effective removal of $Cs^+$ ions from complex aqueous solutions.

Herein, we provide an activation approach to enhance the adsorption performance of layered metal sulfides for the first time, *i.e.* cation-activated layered indium thioantimonates, $K_2In_2Sb_2S_7\cdot 2.2H_2O$ (KIAS), achieving ultra-fast and selective capture of $Cs^+$ ions. KIAS exhibits high radiation stability and good pH durability (pH 1–13), and excellent $Cs^+$ adsorption activity. Compared to unactivated $[(CH_3)_2NH_2]_2In_2Sb_2S_7$ (NIAS), the as-prepared KIAS with large interlayer spacing and labile interlayer $K^+$ ions exhibits extremely fast adsorption kinetics and can remove ~93% of $Cs^+$ ions in only 1 min at room temperature. To our knowledge, it is the fastest for various $Cs^+$ adsorbents reported until now. KIAS displays high exchange capacity of 309.60 mg $g^{-1}$, and can selectively capture $Cs^+$ in the presence of excess interferents such as $Na^+$, $Mg^{2+}$, $CO_3^{2-}$, and humic acid and even in actual tap water or lake water. Furthermore, KIAS can reversibly capture $Cs^+$ and be fully regenerated for at least five adsorption–desorption cycles in an easy-to-operate and environmentally friendly elution procedure.

# 2 Experimental

## 2.1 Chemical materials

All chemical reagents were purchased from commercial sources and used without any further purification. They include $In_2S_3$ (99.99%, Sichuan Xinlong Tellurium Technology Development Co., Ltd), $Sb_2S_3$ (98%, Tianjin Jinhai Huaxing Technology Development Co., Ltd), S (99.5%, Tianjin Kermel Chemical Co., Ltd), dimethylamine solution (33% in water, Sinopharm Chemical Reagent Co., Ltd), methanol (AR, Sinopharm Chemical Reagent Co., Ltd), CsCl (99.99%, Shanghai Longjin Metallic Material Co., Ltd), and KCl (99.9%, Greagent).

## 2.2 Synthesis of NIAS and KIAS

NIAS was fabricated by a modified method according to our previous report.[29] A mixture of $In_2S_3$ (3.258 g, 10.0 mmol), $Sb_2S_3$ (0.849 g, 2.5 mmol), S (0.802 g, 25.0 mmol) in 20 mL dimethylamine (33% in water) and 20 mL methanol was sealed in a stainless-steel reactor with a 235 mL Teflon liner and heated at 160 °C for 6 days. After cooling down to room temperature by natural ventilation, the product was washed several times with deionized water and ethanol and then dried under vacuum at 50 °C. 1.925 g of pure yellow brick-like crystals of NIAS was collected in a yield of 97.49% based on Sb. To activate adsorbents, 0.5 g of NIAS powder was first added into 100 mL of 1 mol $L^{-1}$ CsCl solution and shaken for 2 d at 85 °C, with replacement of CsCl solution once during treatment to obtain a sample labeled Cs@NIAS; Cs@NIAS was then dipped into 100 mL of 2 mol $L^{-1}$ KCl solution and shaken for 2 d at room temperature, with KCl solution replaced once during the process to derive a sample labeled KIAS.

## 2.3 Physical characterization

Energy-dispersive X-ray spectroscopy (EDS), elemental distribution mapping, and field emission scanning electron microscope (SEM) analyses were performed on a JEOL JSM-6700F scanning electron microscope. Transmission electron microscopy (TEM), high-resolution TEM and selected-area electron diffraction (SAED) measurements were performed using FEI Tecnai G2 F20. Elemental analyses (EA, to determine the weight% of N, C, and H) were performed on a German Elementar vario MICRO cube. Thermogravimetric analyses (TGA) were conducted on a Netzsch STA449C from ambient temperature to 600 °C at a heating rate of 10 °C $min^{-1}$ under a nitrogen atmosphere. Powder X-ray diffraction (PXRD) patterns were collected in the $2\theta$ range of 5–65° on a Japan Rigaku Miniflex II diffractometer using a Cu K$\alpha$ X-ray source ($\lambda$ = 1.54178 Å). Ultraviolet-visible (UV-vis) absorption spectra were recorded by a Shimadzu UV-2600 spectrophotometer using a $BaSO_4$ plate as a reference (100% reflectance). The band gap energy was estimated by using the Kubelka–Munk function.[30] X-ray photoelectron spectra (XPS) analyses were carried out on

a ThermoFisher ESCALAB 250Xi XPS spectrometer system with an Al Kα X-ray source. All peaks were referenced to the signature C 1s peak binding energy for adventitious carbon at 284.8 eV. The fitting of the peaks has been done using Avantage 5.932 software. Inductively coupled plasma-optical emission spectrometry (ICP-OES) was performed with a Thermo 7400 and inductively coupled plasma-mass spectrometry (ICP-MS) was studied on an XSeries II to accurately determine the concentration of metal ions.

### 2.4 Radiolytic and hydrolytic stability tests

The γ-ray irradiation experiments were carried out at the no. 1 $^{60}$Co irradiation source (2 000 000 Ci) unit of Suzhou CNNC Huadong Radiation Co., Ltd, China. KIAS was irradiated with two different total doses of 100 kGy (1.05 kGy $h^{-1}$ for 95 h) and 200 kGy (1.05 kGy $h^{-1}$ for 190 h), respectively. The irradiated samples were further analyzed by PXRD patterns and $Cs^+$ adsorption experiments. In hydrolytic stability experiments, KIAS was shaken in $HNO_3$ or NaOH solutions with various pH values from 1 to 13 for 5 h. The pH of all solutions was tested on a Shanghai Leich E-201F pH meter. After solid–liquid separation, the solid samples were analyzed for structural stability by PXRD patterns and the concentration of $In^{3+}$ ions released into the solution was measured by ICP-MS.

### 2.5 Batch adsorption experiments

In this work, ion exchange experiments were carried out by the batch method. A typical $Cs^+$ adsorption experiment was first performed at room temperature by shaking 10 mg of KIAS dispersed in 10 mL of non-radioactive $Cs^+$ aqueous solution ($V/m$ = 1000 mL $g^{-1}$). The mixture was then separated after a contact time of 5 h using a membrane filter with a pore size of 0.22 μm. The concentration of $Cs^+$ (or other metal ions) in the filtrates was measured by ICP-MS and ICP-OES. The solid material after the adsorption process was collected by centrifugation and washed several times with ultrapure water and ethanol, and then dried under vacuum at 50 °C. More details about the equations and instructions for data analysis are provided in the ESI.†

In radiation adsorption experiments, 10 mg of unirradiated, 100 kGy irradiated and 200 kGy irradiated KIAS was added to 10 mL of ~10 and 50 mg $L^{-1}$ $Cs^+$ solutions and shaken at room temperature for 5 h, respectively. In pH-dependent experiments, the pH values of ~5 mg $L^{-1}$ $Cs^+$ solutions were adjusted to a range of 1–13 by using $HNO_3$ or NaOH solutions. In kinetic experiments, 50 mg of NIAS or KIAS was added into 50 mL of ~2 mg $L^{-1}$ $Cs^+$ solution and shaken at room temperature. The mixture was sampled and filtered at different time intervals to test the concentration of $Cs^+$ ions in the solution. In isotherm experiments, different initial concentrations of $Cs^+$ solutions (50–800 mg $L^{-1}$) were prepared separately. Several interference experiments were carried out under different conditions, including in the presence of large amounts of alkali (earth) metal ion chloride salts (NaCl, KCl, RbCl, $MgCl_2$, $CaCl_2$, $SrCl_2$, $BaCl_2$), anionic sodium salts ($Na_2CO_3$, $NaHCO_3$, $NaNO_3$, $Na_2SO_4$), and humic acid (HA, as dissolved organic matter), respectively. In the actual water samples, low concentrations of $Cs^+$ were individually added to local tap water (Gulou District, Fuzhou) and lake water (West Lake, Fuzhou) to simulate $Cs^+$-contaminated water samples. Finally, in adsorption–desorption cycle experiments, 10 mg of KIAS was first added to 10 mL of ~10 or 50 mg $L^{-1}$ $Cs^+$ solutions and shaken continuously for 5 h at room temperature. The suspension was separated by centrifugation and the filtrate was measured for determining the final concentration of $Cs^+$ by ICP-MS. The precipitate was washed with ultrapure water and ethanol, and dried under vacuum at 50 °C. This dried sample was then treated with 0.2 mol $L^{-1}$ KCl solution as an eluent for 5 h, filtered and analyzed using ICP-MS for the amount of $Cs^+$ ions released into the solution. The regeneration of KIAS was investigated by using KCl solution for up to 5 cycles and the same sample was used repeatedly for the uptake of $Cs^+$ ions.

## 3 Results and discussion

### 3.1 Synthesis and activation of NIAS

To improve NIAS yield, our previously reported synthetic method was modified mainly as follows: (i) the reactant molar ratio of $In_2S_3$ : $Sb_2S_3$ : S was adjusted from 1 : 1 : 5 to 4 : 1 : 10; (ii) the mixture of *N*,*N*-dimethylformamide and hydrazine hydrate was replaced by a mixture of dimethylamine and methanol; (iii) the volume of the Teflon liner was increased from 20 mL to 235 mL.[29] The resultant NIAS was isolated as bright-yellow brick-like crystals with a significantly enhanced product yield of 97.49% (1.925 g) with respect to 72% of our previous crystals (0.284 g). The phase purity was characterized by PXRD (Fig. 1a). The structure of NIAS is constitutive of infinite $[In_2Sb_2S_7]_n^{2n-}$ anionic layers with protonated $[(CH_3)_2NH_2]^+$ cations located in interlayer spaces (Fig. 1b). The $[In_2Sb_2S_7]_n^{2n-}$ layer consists of infinite $[In_2Sb_2S_8]_n^{4n-}$ ribbons, which are arranged in an antiparallel mode *via* corner-sharing S atoms (Fig. 1c).

The as-prepared NIAS suffers from poor adsorption kinetics and low removal rates for $Cs^+$ ions, probably due to small interlayer distance and strong N–H···S hydrogen bonding interactions. In this case, we managed to activate NIAS by displacing protonated $[(CH_3)_2NH_2]^+$ with hard $K^+$ ions, but sluggish $[(CH_3)_2NH_2]^+$ could hardly be directly replaced with $K^+$ (Fig. 1d). We then tried activation with relatively soft $Cs^+$ ions and only ~30% of $[(CH_3)_2NH_2]^+$ cations could be substituted out (based on EDS, Fig. S1,† and EA, N = 2.24%, C = 3.98%, H = 1.25%). It is clear that "soft" $Cs^+$ activates the channels more effectively than "hard" $K^+$. This may stem from weak interactions between hard $K^+$ and soft surface $S^{2-}$, which make it difficult for $K^+$ to be directly replace with $[(CH_3)_2NH_2]^+$.[31] Further activation of previously obtained Cs@NIAS with hard $K^+$ showed that both $Cs^+$ and remaining $[(CH_3)_2NH_2]^+$ ions could be replaced, which greatly improves the adsorption performance of the material for $Cs^+$, as will be discussed in detail in the following sections.

### 3.2 Characterization of KIAS

PXRD, elemental mapping, EDS, EA, TGA, TEM, UV-vis and XPS were employed to analyze the activation of $Cs^+$ and $K^+$ ions into

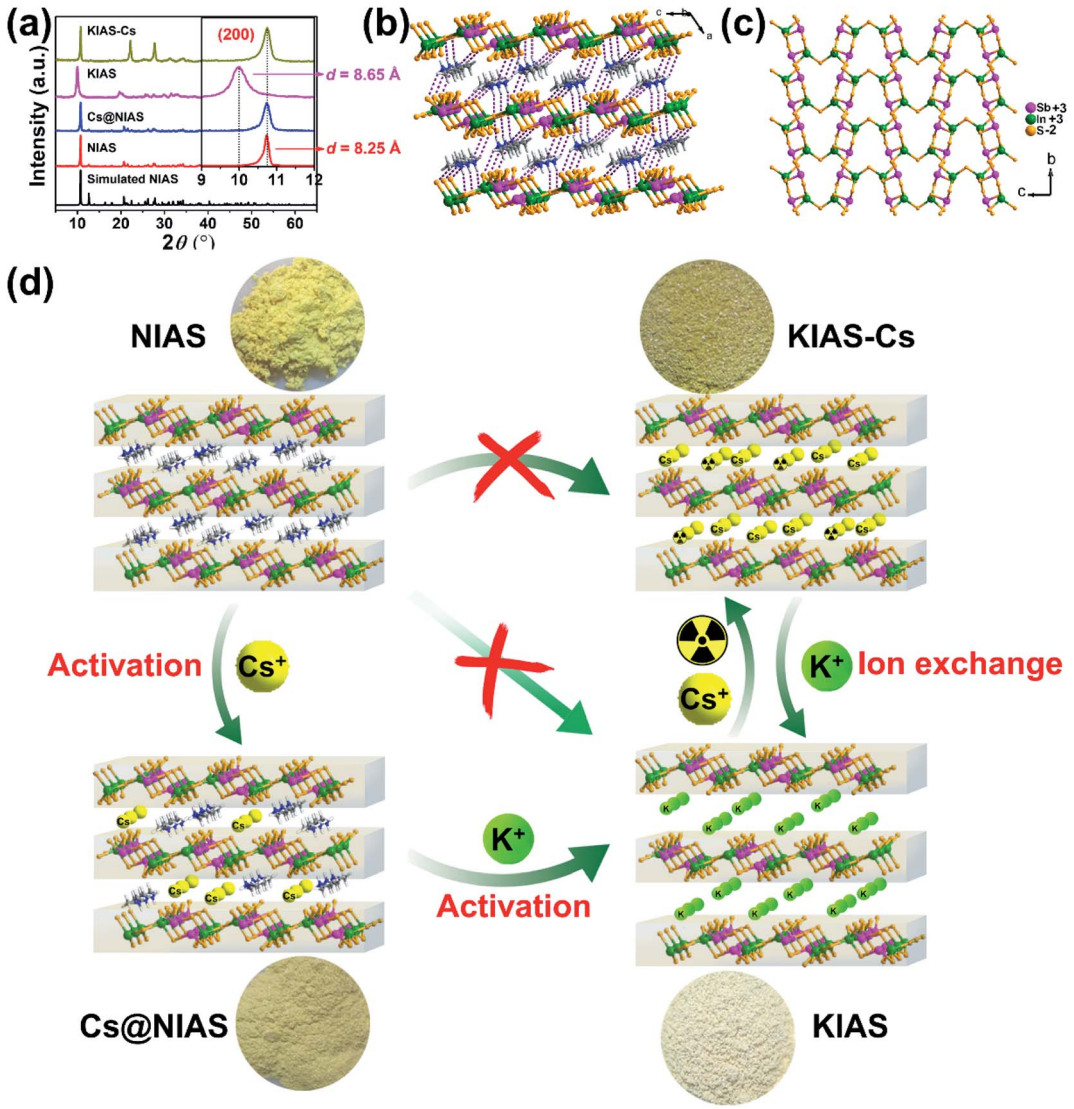


Fig. 1 (a) PXRD patterns of NIAS, Cs@NIAS, KIAS, and KIAS-Cs; inset: magnification of PXRD patterns in the 2$\theta$ range of 9–12°. (b) The stacking of $[In_2Sb_2S_7]_n^{2n-}$ layers with protonated $[(CH_3)_2NH_2]^+$ located in interlayer spaces (H-bonds are represented by deep purple dotted lines). (c) $[In_2Sb_2S_7]_n^{2n-}$ layer viewed along the *a* axis. (d) Schematic representation displaying the activation of NIAS and ion-exchange of KIAS.

NIAS. PXRD pattern results manifest that the layered crystal structure of the pristine sample remains unchanged after the activation processes of $Cs^+$ and $K^+$ ions, with only an expansion of interlayer spacing (Fig. 1a). KIAS exhibits an increased interlayer distance of 8.65 Å compared to 8.25 Å for the host NIAS due to a large amount of $H_2O$ molecules entering the interlayer spaces.[32] The appropriate interlayer spacing and labile interlayer $K^+$ ions give KIAS outstanding ion exchange properties. In the elemental mapping images of Cs@NIAS and KIAS, S, In, Sb, Cs or K are observed, demonstrating successful activation of NIAS by $Cs^+$ and $K^+$ ions (Fig. 2a–c). More intuitive results are observed in EDS analysis (Fig. S1†). The chemical formula of KIAS was derived from EDS, EA (N < 0.3%, C < 0.3%, H = 0.55%) and TGA (2.2% weight loss from room temperature to 500 °C, see Fig. S2†) results to be $K_2In_2Sb_2S_7 \cdot 2.2H_2O$. TEM images demonstrate the typical lamellar morphology and smooth surface of KIAS, and the layers are thinner than those of Cs@NIAS, possibly due to $K^+$-activation resulting in expansion and even exfoliation of layer (Fig. 2d and e). More crystallographic information can be inferred from the SAED patterns (inset, Fig. 2d and e) and high-resolution TEM images (Fig. S3†), which display the crystal fringes of Cs@NIAS and KIAS. The SAED patterns clearly show numerous regularly arranged spots, revealing the single crystalline nature. Optical absorption spectra of NIAS, Cs@NIAS and KIAS are plotted in Fig. 3a. The absorption spectrum of pristine NIAS exhibits a negligible shift after the initial activation of $Cs^+$, while a distinct blueshift is observed from 2.58 eV to 2.66 eV upon further introduction of $K^+$, consistent with their color change (Fig. 1d). This demonstrates that the distance between two layers increases due to activation of $K^+$ not $Cs^+$. XPS spectra show two new characteristic peaks of Cs $3d_{3/2}$ at 738.0 eV and Cs $3d_{5/2}$ at 723.9 eV in Cs@NIAS, and other characteristic peaks of K $2p_{1/2}$ at 295.4 eV and K $2p_{3/2}$ at 292.7 eV also occur in KIAS (Fig. 3b and S4†).

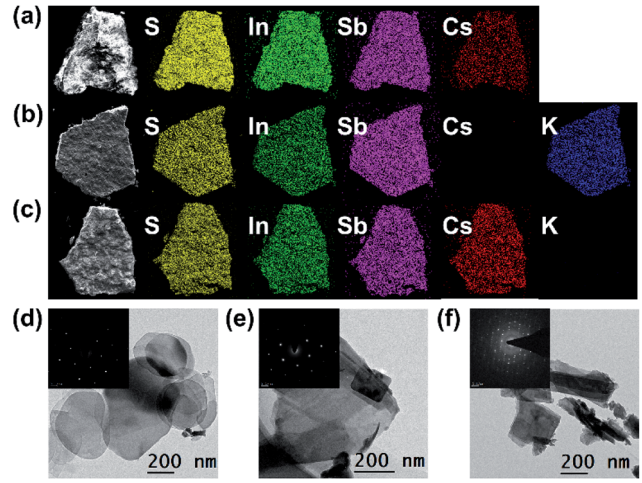


Fig. 2 Elemental mapping images of (a) Cs@NIAS, (b) KIAS, and (c) KIAS-Cs. TEM images of (d) Cs@NIAS, (e) KIAS and (f) KIAS-Cs; inset: the corresponding SAED patterns for d–f.

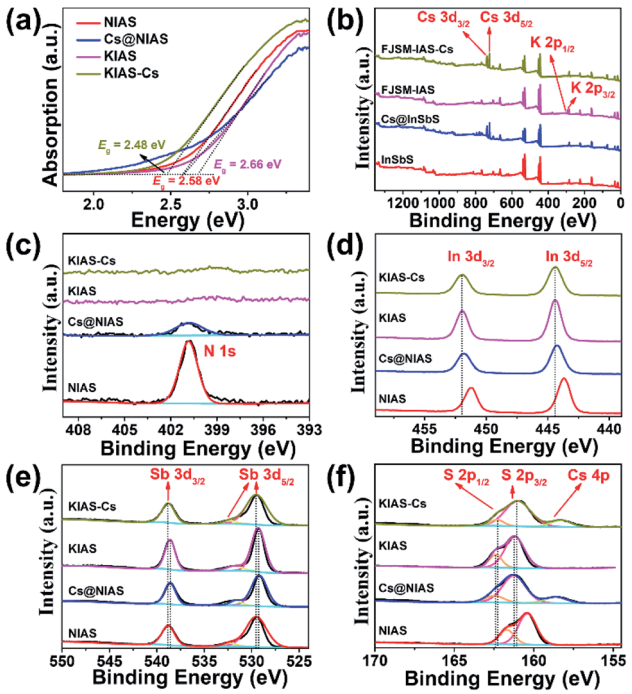


Fig. 3 (a) UV-vis spectra, (b) XPS full survey spectra, (c) high-resolution N 1s spectra, (d) high-resolution In 3d spectra, (e) high-resolution S 2p spectra and (f) high-resolution Sb 3d spectra of NIAS, Cs@NIAS, KIAS and KIAS-Cs.

Moreover, it is worth noting that the characteristic peak of N 1s at 400.8 eV is greatly quenched after exchange of $[(CH_3)_2NH_2]^+$ with $Cs^+$ or $K^+$ in NIAS, indicating complete replacement of $[(CH_3)_2NH_2]^+$ (Fig. 3c).

### 3.3 Characterization of KIAS-Cs

A sample of KIAS solid product immersed in $Cs^+$ solution at a concentration of approximately 3000 mg $L^{-1}$ is denoted as KIAS-Cs, where $V/m$ is 1000 mL $g^{-1}$. PXRD of KIAS-Cs manifests a similar pattern to that of NIAS, characterized by a shift of the (200) Bragg peak towards higher $2\theta$ and a corresponding reduction in the interlayer distance to 8.25 Å compared to those of KIAS (Fig. 1a). Elemental mapping displays a homogeneous distribution of Cs in KIAS-Cs (Fig. 2c). It is worth noting that there is no K element, proving the saturated exchange of $K^+$ with $Cs^+$. As can be observed from Fig. 2f, KIAS-Cs maintains a lamellar structure, while the surface becomes scabrous and bumpy, probably owing to additional surface adsorption.

UV-vis and XPS spectra were measured to further analyze the ion-exchange mechanism of KIAS-Cs. The band gap of KIAS-Cs is shifted to lower energy (2.48 eV) with respect to that of KIAS (Fig. 3a). The redshift in the band gap of KIAS-Cs may be attributed to the stronger bonding interactions of Cs···S than those of K···S.[33] Comparing XPS full survey and high-resolution spectra, two characteristic peaks of Cs $3d_{3/2}$ at 738.0 eV and Cs $3d_{5/2}$ at 723.9 eV appear in KIAS-Cs, while two characteristic peaks of K $2p_{1/2}$ at 295.4 eV and K $2p_{3/2}$ at 292.7 eV disappear (Fig. 3b and S4†). Additionally, the binding energies of In $3d_{3/2}$ at 451.9 eV and In $3d_{5/2}$ at 444.4 eV do not change in KIAS and KIAS-Cs (Fig. 3d). However, the main binding energies of Sb 3d and S 2p shift slightly (Fig. 3e and f). Sb $3d_{3/2}$ increases from 538.6 to 538.9 eV and Sb $3d_{5/2}$ increases from 529.2 eV to 529.5 eV, which suggests a lower electron density around Sb in KIAS-Cs, possibly owing to chemisorption of "soft" $Cs^+$ through the lone pair electrons of $Sb^{3+}$.[34–36] The binding energies of S $3p_{1/2}$ and S $3p_{3/2}$ decrease from 162.4 to 162.3 eV and from 161.2 to 161.1 eV, respectively, manifesting a higher electron density around S in KIAS-Cs.[35,37] The exchange of K with less electronegative Cs leads to a higher electron density around S, probably demonstrating the electron transfer from Cs to S and formation of Cs···S bonding interactions. According to the hard–soft acid–base theory, soft base $S^{2-}$ has a higher affinity for relatively "soft" $Cs^+$ compared to "hard" $K^+$.[34] Therefore, ion exchange between $Cs^+$ and $K^+$ may lead to the formation of strong Cs···S bonding interactions.

### 3.4 Radiolytic and hydrolytic stability and adsorption activity

When treating radioactive wastewater, the adsorbent will be exposed to intense radiation, which may damage its structure leading to reduced adsorption activity of radionuclides. Thus, the development of radiation-stabilized adsorbent materials is of great research importance for the remediation of radionuclides. To evaluate the radiation resistance of KIAS materials, the structural stability and $Cs^+$ capture efficiency of KIAS after γ-ray irradiation at various dose levels (100 or 200 kGy) were systematically studied. As shown in Fig. 4a, PXRD patterns of irradiated KIAS can match well with pristine ones, indicating its excellent radiation resistance. Furthermore, the $Cs^+$ removal rates ($R^{Cs}$) of ~95% show tiny changes between KIAS samples under different doses of γ-irradiation (Fig. 4b and Table S1†). These characteristics provide a set of prerequisites for the practical application of KIAS under extreme conditions of strong radiation fields.

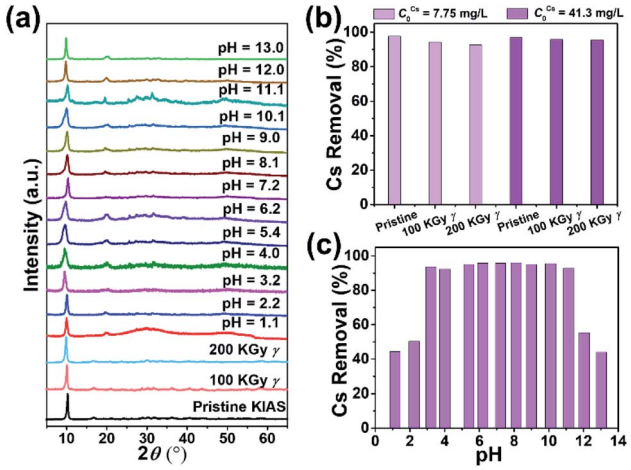


Fig. 4 (a) PXRD patterns of pristine KIAS and the corresponding irradiated samples and $Cs^+$-exchanged products at different pH values. (b) $R^{Cs}$ (%) of pristine KIAS and irradiated samples. (c) $R^{Cs}$ (%) of KIAS at various pH values.

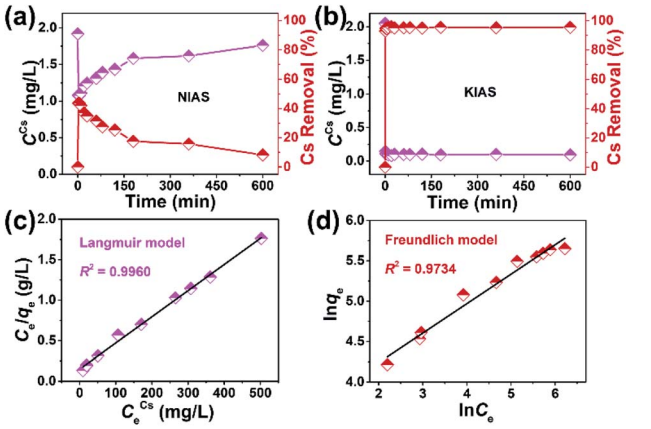


Fig. 5 (a) Adsorption kinetics for $Cs^+$ by (a) unactivated NIAS and (b) KIAS plotted as concentration (mg $L^{-1}$) (purple line) and removal rate (%) (red line) *vs.* time (min). (c) The Langmuir and (d) Freundlich isotherm models of $Cs^+$ adsorption using KIAS.

In addition, to accommodate the change from acidic to alkaline radioactive cesium-containing wastewater, the influence of pH on the chemical stability and $Cs^+$ adsorption activity of KIAS was investigated. Over a wide pH range from 1 to 13, KIAS exhibits a good retention of the pristine structure and crystallinity (Fig. 4a). And as demonstrated in Table S2 and Fig. S5,† the $In^{3+}$ leaching rates ($L^{In}$) of KIAS are almost negligible (≤0.01%), manifesting the excellent chemical stability of KIAS. The effect of initial solution pH on $Cs^+$ removal by KIAS is shown in Fig. 4c and Table S2.† Over a narrow initial pH range (1–3), a substantial increase in $R^{Cs}$ from 44% to 94% is observed. The low $R^{Cs}$ in the acidic region may derive from competitive adsorption behavior between $H_3O^+$ and $Cs^+$.[38,39] With a further rise in initial pH (4 to 11), $R^{Cs}$ can remain at a high constant level (exceeding 92%) and all distribution coefficient ($K_d^{Cs}$) values are above $10^4$ mL $g^{-1}$, demonstrating that the adsorbent KIAS has a strong affinity for $Cs^+$ ions in the pH range of 3–11. Even in a highly alkaline environment (pH = 13.0), >44% of $Cs^+$ ions can be removed by KIAS.

### 3.5 Adsorption kinetics

During the actual sequestration of radionuclides, the extremely fast kinetic rate of sorbents helps to ensure less radiation damage. The decontamination of $Cs^+$ ions by unactivated NIAS and KIAS samples was investigated as a function of time. As shown in Fig. 5a and Table S3,† the adsorption behavior of NIAS for $Cs^+$ is unstable, and although $R^{Cs}$ reaches 43.69% within 2 min, the adsorbed $Cs^+$ ions desorb rapidly, with only 8.24% after 600 min. In contrast, KIAS shows dramatically enhanced adsorption kinetics for $Cs^+$ ions (Fig. 5b and Table S4†). After 1 min of exposure, the $Cs^+$ concentration decreases sharply from 2.05 to 0.144 mg $L^{-1}$, reaching $R^{Cs}$ of ~93% and near equilibrium. Even after 600 min, $R^{Cs}$ of KIAS is more than 95%. The ultra-fast adsorption kinetics of KIAS should be attributed to its large interlayer spacing and easily movable interlayer $K^+$ ions, facilitating rapid exchange of external $Cs^+$ with $K^+$ ions, while the unstable adsorption behavior of NIAS may be due to surface adsorption. Clearly, the cation-activation approach greatly improves the adsorption efficiency of layered metal sulfides for $Cs^+$, while avoiding the release of environmentally unfriendly organic cations during $Cs^+$ incarceration. As tabulated in Table S5,† such an ultra-fast kinetics as well as high removal rate (~93% in 1 min) of KIAS ranks ahead of previously reported well-known $Cs^+$ adsorbents, such as FJSM-SnS (73% in 5 min),[13] KMS-1 (90% in 5 min),[24] KTS-3 (94% in 5 min),[28] K-MPS-1 (78% in 15 min),[40] zeolite A (90% in 90 min),[41] and FJSM-InMOF (91.7% in 3 h).[42]

The kinetic data are fitted using the pseudo-first-order and pseudo-second-order models, which can be expressed according to eqn (S6) and (S7),† respectively. The fitted results are shown in Fig. S6.† The adsorption process for $Cs^+$ on KIAS follows the pseudo-second-order model ($R^2 = 1$) better than the pseudo-first-order model ($R^2 = 0.9998$). The pseudo-second-order model demonstrates that the adsorption process of $Cs^+$ on KIAS involves both physical diffusion and chemisorption, and that chemisorption is the main rate-limiting step.[43]

### 3.6 Adsorption isotherms

To better evaluate the adsorption performance of KIAS for $Cs^+$ ions, a systematic adsorption isotherm study was carried out by varying the $Cs^+$ concentrations in an aqueous solution. The $Cs^+$ adsorption equilibrium data (Table S5†) are linearly fitted with the Langmuir and Freundlich isotherm models, which can be expressed by eqn (S8) and (S9),† respectively. Fig. 5c and d depict fitted straight lines of Langmuir and Freundlich isotherm models for $Cs^+$ removal using KIAS, respectively. The corresponding constants and parameters are presented in Table 1. The adsorption data for KIAS can be well fitted by both Langmuir and Freundlich isotherm models. However, the correlation coefficient of the Langmuir isotherm model ($R^2 \geq 0.9960$) is much higher than that of the Freundlich isotherm model ($R^2 \leq 0.9734$), indicating that the Langmuir isotherm

Table 1 Constants and parameters of the isotherm models describing adsorption of $Cs^+$ onto KIAS

| Langmuir model | | | |
|---|---|---|---|
| $q_m$ (mg $g^{-1}$) | $b$ (L $mg^{-1}$) | $R^2$ | $R_L$ |
| 309.60 | 0.0218 | 0.9960 | 0.0550 |
| **Freundlich model** | | | |
| $n$ | $K_f$ (mg $g^{-1}$)(L $mg^{-1})^{1/n}$ | | $R^2$ |
| 2.7379 | 3222.3299 | | 0.9734 |

model can better describe the adsorption process. The Langmuir isotherm model suggests a monolayer adsorption mechanism of $Cs^+$ on KIAS whose surface is homogeneous.[44] Furthermore, the separation factor ($R_L$) value for the Langmuir isotherm model calculated from eqn (S10) is 0.0550, which means the adsorption process of $Cs^+$ on KIAS is favorable.[45]

The theoretical adsorption capacity of KIAS, assuming that all $K^+$ ions are completely replaced by $Cs^+$ ions, can be calculated from eqn (S11)† to be 325.97 mg $g^{-1}$. The maximum adsorption capacity ($q_m^{Cs}$) of KIAS according to the Langmuir isotherm model is 309.60 mg $g^{-1}$ (Table 1), very close to the theoretical one, which is higher than those of most previously reported adsorbents (*e.g.*, FJSM-GAS-1, KMS-1, KTS-1, $K_4Nb_6O_7$, NaFeTiO, zeolite A, AMP-PAN: 52.8–280 mg $g^{-1}$ for $Cs^+$; Table S6†).[14,24,28,41,46–48]

### 3.7 Effect of coexisting ions and dissolved organic matter

Nuclear wastewater often contains a large excess of non-radioactive interfering ions, such as a high concentration of alkali (earth) metal cations (*e.g.*, $Na^+$, $K^+$, $Mg^{2+}$, $Ca^{2+}$), which can affect the selective capture of $Cs^+$ by adsorbents.[6] There is therefore an urgent demand to investigate the effect of these interfering species on the selective adsorption of $Cs^+$. Competitive adsorption experiments of $Cs^+$ on KIAS in the presence of individual $Na^+$, $K^+$, $Rb^+$, $Mg^{2+}$, $Ca^{2+}$, $Sr^{2+}$ and $Ba^{2+}$ were carried out. As shown in Fig. 6a and Table S7,† KIAS can maintain high $K_d^{Cs}$ values from $3.05 \times 10^3$ to $1.58 \times 10^4$ mL $g^{-1}$. In particular, all $R^{Cs}$ of KIAS are more than 90% in excessive individual $Na^+$, $K^+$, $Rb^+$, $Mg^{2+}$, $Ca^{2+}$, and $Ba^{2+}$ solutions.

The effective uptake of $Cs^+$ from wastewater containing large amounts of $Na^+$ ions has been a serious challenge owing to the similar hydration radii of $Cs^+$ and $Na^+$ (218 pm for $Cs^+$ and 219 pm for $Na^+$).[49] The adsorption performance of KIAS for $Cs^+$ at a variety of Na/Cs molar ratios was investigated. At Na/Cs molar ratios of 12.43–53.31, $K_d^{Cs}$ values can maintain above $10^4$ mL $g^{-1}$ with corresponding $R^{Cs}$ greater than 92% (Fig. 6b and Table S8†). Meanwhile, at the molar ratio (Na/Cs) of 300.78, $K_d^{Cs}$

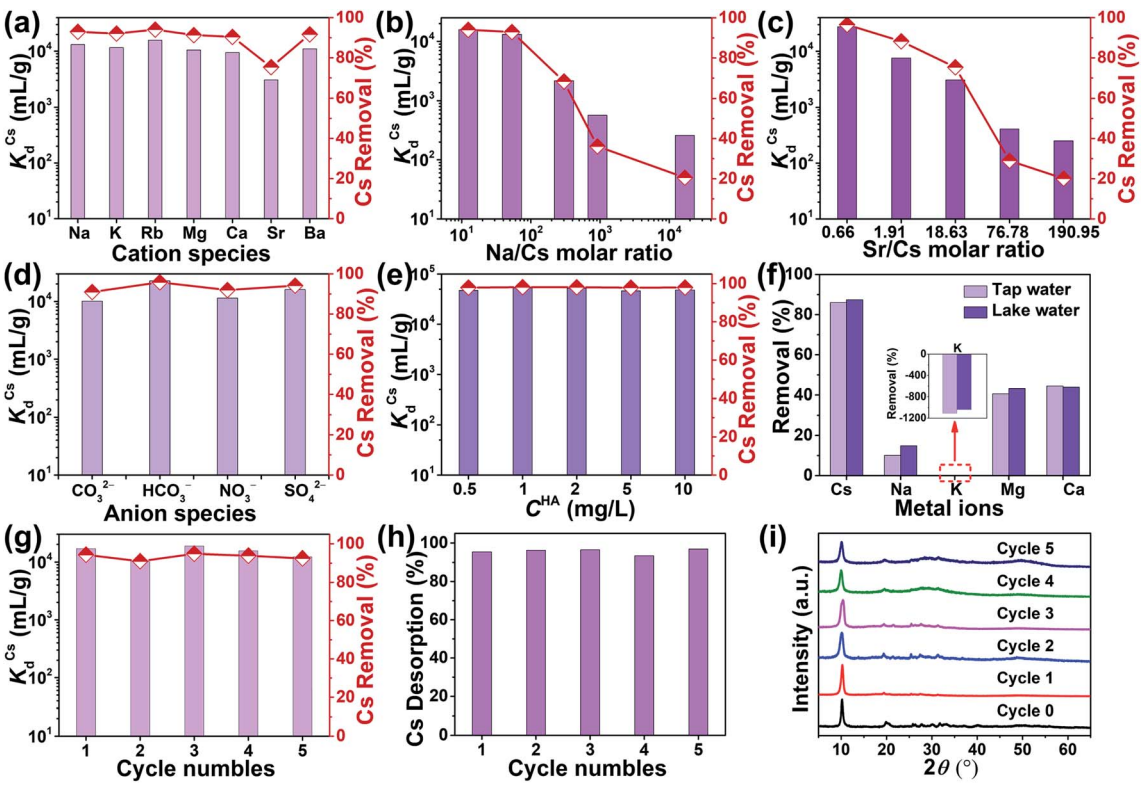


Fig. 6 Variation of $K_d^{Cs}$ values (mL $g^{-1}$) or $R^{Cs}$ (%) of KIAS with (a) various individual alkali or alkaline-earth metal ions, (b) Na/Cs molar ratios, (c) Sr/Cs molar ratios, (d) various individual anions, and (e) 0.5–10 mg $L^{-1}$ HA. (f) $R^{Cs}$ (%) in contaminated tap water and lake water samples. (g) $K_d^{Cs}$ values (mL $g^{-1}$) and $R^{Cs}$ (%) and (h) $Cs^+$ desorption rates (%) for five adsorption–elution cycles ($C_0^{Cs} = 53.016$ mg $L^{-1}$). (i) PXRD patterns for pristine KIAS and its regenerated products in each cycle.

values and $R^{Cs}$ are still as high as $2.16 \times 10^3$ mL $g^{-1}$ and 68.32%, respectively. Even in the presence of a tremendous excess of $Na^+$ ($1.68 \times 10^4$ times), $K_d^{Cs}$ value is $2.59 \times 10^2$ mL $g^{-1}$. High $K_d^{Cs}$ values and $R^{Cs}$ indicate that KIAS still exhibits good $Cs^+$ capture in competitive environments, making it significantly better than traditional inorganic exchange materials such as titanosilicates, or commercial scavengers such as AMP-PAN.[48,50]

What's more, $^{90}Sr$ is also a major hazardous fission byproduct of U in nuclear reactors.[5] Therefore, we also performed $Cs^+$-competitive experiments of KIAS in the presence of excess $Sr^{2+}$. As shown in Fig. 6c and Table S9,† at Sr/Cs molar ratios of 0.66–18.63, $K_d^{Cs}$ values and $R^{Cs}$ of KIAS increase from $3.05 \times 10^3$ to $2.77 \times 10^4$ mL $g^{-1}$ and from 75.33 to 96.51%, respectively. When the Sr/Cs molar ratio is increased by ~500 times, $K_d^{Cs}$ value still amounts to $2.51 \times 10^2$ mL $g^{-1}$. This indicates that the KIAS ion-exchanger has excellent selectivity for $Cs^+$ ions.

Considering the wide distribution of anions such as $CO_3^{2-}$, $HCO_3^-$, $NO_3^-$, and $SO_4^{2-}$ in various water systems, we investigated the influence of their coexistence on the $Cs^+$ uptake. The results are shown in Fig. 6d and Table S10.† High $K_d^{Cs}$ values ($1.01 \times 10^4$ to $2.27 \times 10^4$ mL $g^{-1}$) and $R^{Cs}$ (90.99–95.78%) are obtained with the coexistence of different anions and $Cs^+$ ions. In particular, in the presence of $HCO_3^-$, $R^{Cs}$ of KIAS can exceed 95%. It is clear that the common $CO_3^{2-}$, $HCO_3^-$, $NO_3^-$, and $SO_4^{2-}$ anions appear to have little influence on the uptake of $Cs^+$ ions.

In addition to inorganic ions, natural dissolved organic matter in contaminated liquid may also affect the capture performance of KIAS for $Cs^+$. Humic acid (HA) is an organic substance, containing functional groups such as –COOH, –OH and $–NH_2$, which can form polymers in solution and has strong complexation.[51] HA was chosen as a representative of dissolved organic matter in this work. The effect of different amounts of HA on the adsorption of $Cs^+$ by KIAS is shown in Fig. 6e and Table S11.† The results show that as the concentration of HA increases, $K_d^{Cs}$ values and $R^{Cs}$ do not decrease, but both remain at a high level. For example, when the concentrations of HA and $Cs^+$ reach around 10 and 5 mg $L^{-1}$, respectively, greater than 97% of $Cs^+$ can still be captured. Obviously, HA has little effect on $Cs^+$ adsorption under the test conditions, probably because of the weak complexation between HA and $Cs^+$ ions.[52]

### 3.8 $Cs^+$ ion capture in actual water environments

To gauge the combined effects of actual contaminated water, tap water and lake water spiked with low concentration $Cs^+$ were sampled to further test the $Cs^+$ removal. The adsorption results of KIAS on $Cs^+$, $Na^+$, $K^+$, $Mg^{2+}$ and $Ca^{2+}$ are presented in Fig. 6f and Table S12.† $R^{Cs}$ can reach 85.99% in tap water and 87.41% in lake water, much higher than corresponding $R^{Na}$, $R^K$, $R^{Mg}$ and $R^{Ca}$. It should be noted that $R^K$ is negative, *i.e.*, there are more $K^+$ ions in the solution after adsorption due to the release of interlayer $K^+$ ions from KIAS during the adsorption process. This proves that KIAS maintains the outstanding selectivity for $Cs^+$ ions even in a complicated environment with $Na^+$, $K^+$, $Mg^{2+}$ and $Ca^{2+}$ ions.

### 3.9 Desorption and regeneration

Easy desorption and renewability of adsorbent are an important factor in evaluating the cost of radioactive waste disposal in practical applications. In addition to the ultra-fast kinetics, excellent adsorption capacity and high selectivity, KIAS can be regenerated multiple times by a simple and efficient elution procedure with KCl solution. The reusability of this material was systematically investigated for five consecutive adsorption–desorption cycles using 53.016 mg $L^{-1}$ $Cs^+$ solution and 0.2 mol $L^{-1}$ KCl eluent. The removal rate ($R^{Cs}$) and desorption rate ($D^{Cs}$) results are presented in Fig. 6g and h and Table S13.† In the first cycle, KIAS achieves $R^{Cs}$ of more than 94%. Even after the fifth cycle, $R^{Cs}$ is still higher than 92% (Fig. 6g). The desorption rates of $Cs^+$-loaded KIAS after five cycles remain at ~95% (Fig. 6h). Similar results are also obtained using other concentrations of $Cs^+$ solution such as 7.152 mg $L^{-1}$ (Table S13†). High desorption rates obtained by elution using KCl solution in each cycle can also be further verified by elemental distribution mapping and EDS results (Fig. S7 and S8†). Furthermore, SEM images show that the size of KIAS gradually becomes smaller with increasing number of regeneration cycle (Fig. S9†). However, PXRD patterns of regenerated KIAS match well with pristine ones, which indicates that KIAS can maintain its layer structure without collapse after multiple regenerations (Fig. 6i). This can be verified by the very low $In^{3+}$ leaching rates (Table S13†).

### 3.10 Adsorption mechanism

The mechanism of $Cs^+$ uptake by KIAS is clearly revealed through batch adsorption experiments and multiple characterizations. First, the kinetic data follow the pseudo-second-order model, demonstrating that the adsorption process of $Cs^+$ on KIAS involves both physical diffusion and chemisorption, and that the adsorption rate is controlled by a chemical reaction.[43] Second, the Langmuir model fits well with the adsorption isotherm data, indicating a monolayer adsorption mechanism of $Cs^+$ on KIAS with one-molecule/ion thickness adsorption on a homogeneous surface.[44] And the separation factor value ($0 < R_L < 1$) shows favorable adsorption of $Cs^+$ on KIAS.[45] Third, the uniform distribution and adsorption amount of $Cs^+$ on KIAS are visually observed by elemental mapping and EDS analysis, and it can be inferred that $K^+$ ions located in interlayer spaces have been completely replaced by $Cs^+$. Fourth, PXRD patterns show that the interlayer spacing of KIAS-Cs is reduced to 8.25 Å compared to 8.65 Å for KIAS, which is due to $K^+$ ions being replaced by $Cs^+$, carrying a large number of $H_2O$ molecules out of the interlayer spaces.[32] Fifth, optical absorption spectra indicate that the redshift of the KIAS-Cs band gap is probably due to the stronger bonding interactions of Cs···S than those of K···S.[33] Finally, XPS spectra reveal that after adsorption of $Cs^+$, the lower electron density around Sb may result from the chemisorption of "soft" $Cs^+$ *via* the lone pair of electrons of $Sb^{3+}$,[34–36] while the higher electron density around S may be due to the exchange of less electronegative Cs with K, resulting in electron transfer from Cs to S and formation of Cs···S bonding interactions.[35,37] Overall, the adsorption mechanism of $Cs^+$ on KIAS can be concluded as

follows: owing to stronger Cs···S bonding interactions than K···S, $K^+$ located between $[In_2Sb_2S_7]_n^{2n-}$ anionic layers can be exchanged with $Cs^+$.

# 4 Conclusions

The ultra-fast and selective elimination of $Cs^+$ from complicated aqueous solutions has been achieved through the ion exchange method by employing a layered potassium indium thioantimonate, $K_2In_2Sb_2S_7 \cdot 2.2H_2O$ (KIAS), which is activated by cationic substitution from $[(CH_3)_2NH_2]_2In_2Sb_2S_7$ (NIAS). KIAS possesses excellent radiation resistance and good pH durability (pH 1–13), and exhibits high adsorption activity and capacity (309.60 mg $g^{-1}$) towards $Cs^+$. In particular, KIAS achieves top-level adsorption kinetics towards $Cs^+$ with a removal rate of ~93% in only 1 min with respect to unactivated NIAS. High selectivity of $Cs^+$ capture against $Na^+$, $K^+$, $Mg^{2+}$, $Ca^{2+}$, $CO_3^{2-}$, $HCO_3^-$, $NO_3^-$, $SO_4^{2-}$, and humic acid, and even in contaminated tap water or lake water is confirmed by competitive adsorption experiments. We further find that the $Cs^+$-loaded KIAS can be easily regenerated by gentle elution and maintain high removal and desorption rates of $Cs^+$ after 5 adsorption–elution cycles. Batch adsorption experiments combined with multiple characterizations reveal that the adsorption mechanism of $Cs^+$ ions on KIAS is ion exchange between $Cs^+$ and $K^+$ ions located in $[In_2Sb_2S_7]_n^{2n-}$ interlayer spaces. In summary, this work not only presents an effective approach for improving the adsorption performance, *i.e.* cation activation, but also sheds light on the utilization of layered metal sulfides as effective exchangers for decontamination of $^{137}Cs$ from complex wastewater.

# Conflicts of interest

There are no conflicts to declare.

# Acknowledgements

This work was supported by the financial support provided by the National Natural Science Foundation of China (grant no. U21A20296, 22076185, and 21771183) and the Natural Science Foundation of Fujian Province (grant no. 2020J06033).

# References

1 H. R. Yu, J. Q. Hu, Z. Liu, X. J. Ju, R. Xie, W. Wang and L. Y. Chu, Ion-recognizable hydrogels for efficient removal of cesium ions from aqueous environment, *J. Hazard. Mater.*, 2017, **323**, 632–640.
2 A. M. Emara, F. H. El-Sweify, S. F. Abo-Zahra, A. I. Hashim and T. E. Siyam, Removal of Cs-137 and Sr-90 from reactor actual liquid waste samples using a new synthesized bionanocomposite-based carboxymethylcellulose, *Radiochim. Acta*, 2019, **107**, 695–711.
3 S. Kwon, Y. Kim and Y. Roh, Cesium removal using acid- and base-activated biotite and illite, *J. Hazard. Mater.*, 2021, **401**, 123319.
4 K. X. Wang, H. Ma, S. Y. Pu, C. Yan, M. T. Wang, J. Yu, X. K. Wang, W. Chu and Z. Anatoly, Hybrid porous magnetic bentonite–chitosan beads for selective removal of radioactive cesium in water, *J. Hazard. Mater.*, 2019, **362**, 160–169.
5 E. S. Dragan, D. Humelnicu, M. Ignat and C. D. Varganici, Superadsorbents for strontium and cesium removal enriched in amidoxime by a homo-IPN strategy connected with porous silica texture, *ACS Appl. Mater. Interfaces*, 2020, **12**, 44622–44638.
6 H.-M. Yang, C. W. Park, I. Kim and I.-H. Yoon, Hollow flower-like titanium ferrocyanide structure for the highly efficient removal of radioactive cesium from water, *Chem. Eng. J.*, 2020, **392**, 123713.
7 J.-i. Kakehi, E. Kamio, R. Takagi and H. Matsuyama, $Cs^+$ rejection behavior of polyamide RO membranes for feed solutions with extremely low salt concentrations, *Ind. Eng. Chem. Res.*, 2015, **54**, 8782–8788.
8 T. P. Valsala, M. S. Sonavane, S. G. Kore, N. L. Sonar, V. De, Y. Raghavendra, S. Chattopadyaya, U. Dani, Y. Kulkarni and R. D. Changrani, Treatment of low level radioactive liquid waste containing appreciable concentration of TBP degraded products, *J. Hazard. Mater.*, 2011, **196**, 22–28.
9 C. Xu, J. Wang and J. Chen, Solvent extraction of strontium and cesium: A review of recent progress, *Solvent Extr. Ion Exch.*, 2012, **30**, 623–650.
10 F. Chitry, S. Pellet-Rostaing, L. Nicod, J. L. Gass, J. Foos, A. Guy and M. Lemaire, Cesium/sodium separation by nanofiltration–complexation in aqueous medium, *Sep. Sci. Technol.*, 2001, **36**, 1053–1066.
11 A. G. Chmielewski and M. Harasimowicz, Application of ultrafiltration and complexation to the treatment of low-level radioactive effluents, *Sep. Sci. Technol.*, 1995, **30**, 1779–1789.
12 L. Zhou, M. Y. Xu, J. Yin, R. J. Shui, S. Yang and D. B. Hua, Dual ion-imprinted mesoporous silica for selective adsorption of U(VI) and Cs(I) through multiple interactions, *ACS Appl. Mater. Interfaces*, 2021, **13**, 6322–6330.
13 X. H. Qi, K. Z. Du, M. L. Feng, J. R. Li, C. F. Du, B. Zhang and X. Y. Huang, A two-dimensionally microporous thiostannate with superior $Cs^+$ and $Sr^{2+}$ ion-exchange property, *J. Mater. Chem. A*, 2015, **3**, 5665–5673.
14 M. L. Feng, D. Sarma, Y. J. Gao, X. H. Qi, W. A. Li, X. Y. Huang and M. G. Kanatzidis, Efficient removal of $[UO_2]^{2+}$, $Cs^+$, and $Sr^{2+}$ ions by radiation-resistant gallium thioantimonates, *J. Am. Chem. Soc.*, 2018, **140**, 11133–11140.
15 G. Crini and E. Lichtfouse, Advantages and disadvantages of techniques used for wastewater treatment, *Environ. Chem. Lett.*, 2019, **17**, 145–155.
16 D. Alby, C. Charnay, M. Heran, B. Prelot and J. Zajac, Recent developments in nanostructured inorganic materials for sorption of cesium and strontium: Synthesis and shaping, sorption capacity, mechanisms, and selectivity-A review, *J. Hazard. Mater.*, 2018, **344**, 511–530.
17 J. H. Tang, H. Y. Sun, W. Ma, M. L. Feng and X. Y. Huang, Recent progress in developing crystalline ion exchange materials for the removal of radioactive ions, *Chin. J. Struct. Chem.*, 2020, **39**, 2157–2171.

18 A. Clearfield, Inorganic ion exchangers, past, present, and future, *Solvent Extr. Ion Exch.*, 2000, **18**, 655–678.
19 W. He, K. Ai, X. Ren, S. Wang and L. Lu, Inorganic layered ion-exchangers for decontamination of toxic metal ions in aquatic systems, *J. Mater. Chem. A*, 2017, **5**, 19593–19606.
20 B. R. Figueiredo, S. P. Cardoso, I. Portugal, J. Rocha and C. M. Silva, Inorganic ion exchangers for cesium removal from radioactive wastewater, *Sep. Purif. Rev.*, 2018, **47**, 306–336.
21 M. J. Manos and M. G. Kanatzidis, Metal sulfide ion exchangers: superior sorbents for the capture of toxic and nuclear waste-related metal ions, *Chem. Sci.*, 2016, **7**, 4804–4824.
22 X. Zeng, M. Zeng, T. Zhang, P.-W. Cai, M.-L. Feng and X.-Y. Huang, Efficient uptake of uranium(VI) by a layered manganese thiophosphite intercalated with $NH_4^+$, *Chem. Eng. J.*, 2022, **429**, 132474.
23 L. N. Nie and Q. C. Zhang, Recent progress in crystalline metal chalcogenides as efficient photocatalysts for organic pollutant degradation, *Inorg. Chem. Front.*, 2017, **4**, 1953–1962.
24 M. J. Manos and M. G. Kanatzidis, Highly efficient and rapid $Cs^+$ uptake by the layered metal sulfide $K_{2x}Mn_xSn_{3-x}S_6$ (KMS-1), *J. Am. Chem. Soc.*, 2009, **131**, 6599–6607.
25 M. J. Manos, K. Chrissafis and M. G. Kanatzidis, Unique pore selectivity for $Cs^+$ and exceptionally high $NH_4^+$ exchange capacity of the chalcogenide material $K_6Sn[Zn_4Sn_4S_{17}]$, *J. Am. Chem. Soc.*, 2006, **128**, 8875–8883.
26 N. Ding and M. G. Kanatzidis, Selective incarceration of caesium ions by Venus flytrap action of a flexible framework sulfide, *Nat. Chem.*, 2010, **2**, 187–191.
27 J. L. Mertz, Z. H. Fard, C. D. Malliakas, M. J. Manos and M. G. Kanatzidis, Selective removal of $Cs^+$, $Sr^{2+}$, and $Ni^{2+}$ by $K_{2x}Mg_xSn_{3-x}S_6$ ($x = 0.5$–1) (KMS-2) relevant to nuclear waste remediation, *Chem. Mater.*, 2013, **25**, 2116–2127.
28 D. Sarma, C. D. Malliakas, K. S. Subrahmanyam, S. M. Islama and M. G. Kanatzidis, $K_{2x}Mg_xSn_{3-x}S_6$ ($x = 0.65$–1): A new metal sulfide for rapid and selective removal of $Cs^+$, $Sr^{2+}$ and $UO_2^{2+}$ ions, *Chem. Sci.*, 2016, **7**, 1121–1132.
29 K.-Y. Wang, M.-L. Feng, D.-N. Kong, S.-J. Liang, L. Wu and X.-Y. Huang, Layered indium chalcogenidoantimonates $[Me_2NH_2]_2In_2Sb_2S_{7-x}Se_x$ ($x = 0$, 2.20, 4.20, 7) with tunable band gaps and photocatalytic properties, *CrystEngComm*, 2012, **14**, 90–94.
30 W. W. Wendlandt and H. G. Hecht, *Reflectance Spectroscopy*, Interscience Publishers-John Wiley & Sons, Inc., New York, 1966.
31 H. Yang, M. Luo, L. Luo, H. Wang, D. Hu, J. Lin, X. Wang, Y. Wang, S. Wang, X. Bu, P. Feng and T. Wu, Highly selective and rapid uptake of radionuclide cesium based on robust zeolitic chalcogenide *via* stepwise ion-exchange strategy, *Chem. Mater.*, 2016, **28**, 8774–8780.
32 E. R. Nightingale, Phenomenological theory of ion solvation. effective radii of hydrated ions, *J. Phys. Chem.*, 1959, **63**, 1381–1387.
33 M. J. Manos, C. D. Malliakas and M. G. Kanatzidis, Heavy-metal-ion capture, ion-exchange, and exceptional acid stability of the open-framework chalcogenide $(NH_4)_4In_{12}Se_{20}$, *Chem.–Eur. J.*, 2007, **13**, 51–58.
34 R. G. Pearson, Hard and soft acids and bases, *J. Am. Chem. Soc.*, 1963, **85**, 3533–3539.
35 T. J. Whittles, *Electronic Characterisation of Earth-Abundant Sulphides for Solar Photovoltaics*, Springer, 2018.
36 S. Yashonath, P. K. Basu, A. Srinivasan, M. S. Hedge and C. N. R. Rao, Photoelectron spectroscopic studies of the adsorption of organic molecules with lone pair orbitals on transition metal surfaces, *Proc. - Indian Acad. Sci., Chem. Sci.*, 1982, **91**, 101–128.
37 C. Yang and K. Cho, Rapid and selective removal of $Cs^+$ from water by layered potassium antimony thiostannate, *J. Hazard. Mater.*, 2021, **403**, 124105.
38 M. R. Awual, T. Yaita, Y. Miyazaki, D. Matsumura, H. Shiwaku and T. Taguchi, A reliable hybrid adsorbent for efficient radioactive cesium accumulation from contaminated wastewater, *Sci. Rep.*, 2016, **6**, 19937.
39 D. Karamanis and P. A. Assimakopoulos, Efficiency of aluminum-pillared montmorillonite on the removal of cesium and copper from aqueous solutions, *Water Res.*, 2007, **41**, 1897–1906.
40 E. Rathore, P. Pal and K. Biswas, Reversible and efficient sequestration of cesium from water by the layered metal thiophosphate $K_{0.48}Mn_{0.76}PS_3 \cdot H_2O$, *Chem.–Eur. J.*, 2017, **23**, 11085–11092.
41 A. M. El-Kamash, Evaluation of zeolite A for the sorptive removal of $Cs^+$ and $Sr^{2+}$ ions from aqueous solutions using batch and fixed bed column operations, *J. Hazard. Mater.*, 2008, **151**, 432–445.
42 Y. J. Gao, M. L. Feng, B. Zhang, Z. F. Wu, Y. Song and X. Y. Huang, An easily synthesized microporous framework material for the selective capture of radioactive $Cs^+$ and $Sr^{2+}$ ions, *J. Mater. Chem. A*, 2018, **6**, 3967–3976.
43 Y. S. Ho and G. McKay, Pseudo-second order model for sorption processes, *Process Biochem.*, 1999, **34**, 451–465.
44 I. Langmuir, The adsorption of gases on plane surfaces of glass, mica and platinum, *J. Am. Chem. Soc.*, 1918, **40**, 1361–1403.
45 H. Faghihian, M. Iravani, M. Moayed and M. Ghannadi-Maragheh, Preparation of a novel PAN–zeolite nanocomposite for removal of $Cs^+$ and $Sr^{2+}$ from aqueous solutions: Kinetic, equilibrium, and thermodynamic studies, *Chem. Eng. J.*, 2013, **222**, 41–48.
46 J. Sun, D. Yang, C. Sun, L. Liu, S. Yang, Y. Jia, R. Cai and X. Yao, Potassium niobate nanolamina: A promising adsorbent for entrapment of radioactive cations from water, *Sci. Rep.*, 2014, **4**, 07313.
47 P. Amesh, A. S. Suneesh, K. A. Venkatesan, R. U. Maheswari and S. Vijayalakshmi, Preparation and ion exchange studies of cesium and strontium on sodium iron titanate, *Sep. Purif. Technol.*, 2020, **238**, 116393.
48 Y. Park, Y. C. Lee, W. S. Shin and S. J. Choi, Removal of cobalt, strontium and cesium from radioactive laundry wastewater by ammonium molybdophosphate–polyacrylonitrile (AMP–PAN), *Chem. Eng. J.*, 2010, **162**, 685–695.

49 Y. Marcus, A simple empirical model describing the thermodynamics of hydration of ions of widely varying charges, sizes, and shapes, *Biophys. Chem.*, 1994, **51**, 111–127.
50 H. Liu, A. Yonezawa, K. Kumagai, M. Sano and T. Miyake, Cs and Sr removal over highly effective adsorbents ETS-1 and ETS-2, *J. Mater. Chem. A*, 2015, **3**, 1562–1568.
51 O. Celebi, A. Kilikli and H. N. Erten, Sorption of radioactive cesium and barium ions onto solid humic acid, *J. Hazard. Mater.*, 2009, **168**, 695–703.
52 L. Qiu, K. Scott and S. Rousseau, Kinetic and equilibrium studies of Cs(I), Sr(II) and Eu(III) adsorption on a natural sandy soil, *Radiochim. Acta*, 2018, **107**, 55–66.